CHEMISTRY
A EUROPEAN JOURNAL

Lewis Adducts of the Side-On End-On Dinitrogen-Bridged Complex $[\{(NPN)Ta\}_2(\mu\text{-}H)_2(\mu\text{-}\eta^1{:}\eta^2\text{-}N_2)]$ with $AlMe_3$, $GaMe_3$, and $B(C_6F_5)_3$: Synthesis, Structure, and Spectroscopic Properties

Felix Studt,[a] Bruce A. MacKay,[b] Samuel A. Johnson,[b] Brian O. Patrick,[b] Michael D. Fryzuk,*[b] and Felix Tuczek*[a]

Dedicated to Professor W. Preetz on the occasion of his 70th birthday

Abstract: Reaction of the side-on end-on dinitrogen complex $[\{(NPN)Ta\}_2(\mu\text{-}H)_2(\mu\text{-}\eta^1{:}\eta^2\text{-}N_2)]$ (**1**; in which NPN = $(PhNSiMe_2CH_2)_2PPh$), with the Lewis acids XR_3 results in the adducts $[\{(NPN)Ta\}_2(\mu\text{-}H)_2(\mu\text{-}\eta^1{:}\eta^2\text{-}NNXR_3)]$, $XR_3 = GaMe_3$ (**2**), $AlMe_3$ (**3**), and $B(C_6F_5)_3$ (**4**). The solid-state molecular structures of **2**, **3**, and **4** demonstrate that the N–N bond length increases relative to those found in **1** by 0.036, 0.043, and 0.073 Å, respectively. In solution complexes **2**–**4** are fluxional as evidenced by variable-temperature ^1H NMR spectroscopy. The $^{15}N\{^1H\}$ NMR spectra of **2**–**4** are reported; furthermore, their vibrational properties and electronic structures are evaluated. The vibrational structures are found to be closely related to that of the parent complex **1**. Detailed spectroscopic analysis on **2**–**4** leads to the identification of the theoretically expected six normal modes of the Ta_2N_2 core. On the basis of experimental frequencies and the QCB-NCA procedure, the force constants are determined. Importantly, the N–N force constant decreases from 2.430 mdyn Å^{-1} in **1** to 1.876 (**2**), 1.729 (**3**), and 1.515 mdyn Å^{-1} (**4**), in line with the sequence of N–N bond lengths determined crystallographically. DFT calculations on a generic model of the Lewis acid adducts **2**–**4** reveal that the major donor interaction between the terminal nitrogen atom and the Lewis acid is mediated by a σ/π hybrid molecular orbital of N_2, corresponding to a σ bond. Charge analysis performed for the adducts indicates that the negative charge on the terminal nitrogen atom of the dinitrogen ligand increases with respect to **1**. The lengthening of the N–N bond observed for the Lewis adducts is therefore explained by the fact that charge donation from the complex fragment into the π* orbitals of dinitrogen is increased, while electron density from the N–N bonding orbitals p_σ and π_h is withdrawn due to the σ interaction with the Lewis acid.

Keywords: density functional calculations · dinitrogen complexes · nitrogen fixation · Raman spectroscopy · tantalum

Introduction

Although molecular nitrogen (N_2) is not a particularly good ligand, it can bind to transition metal and f-element complexes under certain conditions.[1] Once coordinated N_2 can undergo a number of different transformations that result in functionalization and, in rare cases, cleavage[2] of the N–N bond. The most common reactivity type involves reactions of coordinated dinitrogen with electrophiles. A particularly well-studied process is the reaction of coordinated N_2 with the simplest electrophile, H^+.[3] The impetus for this research has stemmed largely from interest in the biological fixation of N_2 by nitrogenase enzymes,[4] a process that involves interaction of dinitrogen with protons and electrons to generate ammonia in a manner that is still unknown.[5] Protonation studies with various molybdenum complexes span almost three decades[6] and have provided a wealth of data that not only models the conversion of N_2 to NH_3, but has also spun off new processes that have led to stoichio-

[a] F. Studt, Prof. F. Tuczek
Institut für Anorganische Chemie
Christian Albrechts Universität Kiel
Ohlshausenstr. 40, 24098 Kiel (Germany)
Fax: (+49) 431-880-1520
E-mail: ftuczek@ac.uni-kiel.de

[b] Dr. B. A. MacKay, S. A. Johnson, B. O. Patrick, Prof. M. D. Fryzuk
Department of Chemistry, University of British Columbia
Vancouver, B.C. V6T 1Z1 (Canada)
Fax: (+1) 604-822-2847
E-mail: fryzuk@chem.ubc.ca

DOI: 10.1002/chem.200400641

metric formation of organonitrogen derivatives including simple N-heterocycles.[7] These mononuclear dinitrogen complexes of Mo, with the general formula $[L_nMo{-}N_2]$, feature dinitrogen in the end-on mode. The reactivity of bimetallic complexes that incorporate dinitrogen in other bonding modes with Lewis or Brønsted acids is less studied.[8–10]

We recently reported the ditantalum complex $[\{(NPN)Ta\}_2(\mu\text{-}H)_2(\mu\text{-}\eta^1{:}\eta^2\text{-}N_2)]$ (**1**) that binds dinitrogen in the unique side-on end-on mode.[11,12] As a result of this

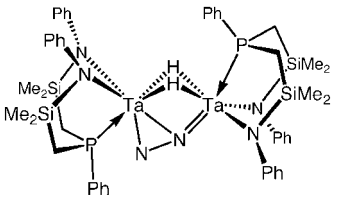

1

type of activation, the N_2 unit of **1** undergoes unprecedented transformations with simple hydride reagents such as 9-borabicyclo[3.3.1]nonane[13] and silanes,[14] which involve addition of H–B or H–Si bonds across the Ta–N π bond [Eq. (1)]. These reactions functionalize the coordinated N_2 unit, forming a new covalent N–B or N–Si bond, and ultimately lead to cleavage of the N–N bond. In this work we detail another type of reactivity that involves adduct formation of the dinitrogen moiety with neutral Lewis acids of Group 13 elements [Eq. (2)].

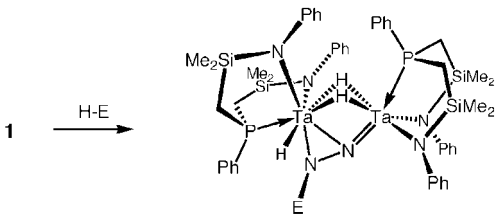

H-E = H-B(C_8H_{14}), H-SiH_2Bu, H-SiH_2Ph (1)

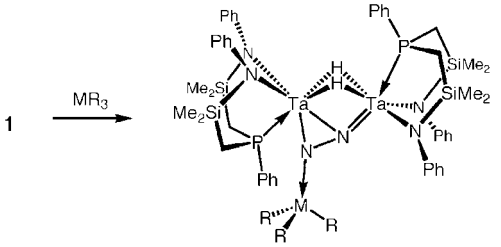

MR_3 = $GaMe_3$ (**2**), $AlMe_3$ (**3**), $B(C_6F_5)_3$ (**4**) (2)

Previous theoretical studies were carried out on complex **1** in order to characterize the electronic structure and the spectroscopic properties of side-on end-on bridging dinitrogen.[12,15] It was found that this ligand carries a negative charge of −1.1 that is equally distributed over the two nitrogen atoms. This charge is lower than found in a related side-on dinitrogen-bridged complex,[16] suggesting a lower degree of activation of N_2 in the side-on end-on mode. Orbital analysis, however, revealed that the terminal nitrogen atom makes higher contributions to the π* and lower contributions to the π orbitals of N_2 than the bridging atom, possibly giving rise to an increased reactivity of the terminal N atom towards electrophiles.[15] Isosurfaces calculated for the two π* orbitals of **1** that correspond to HOMO and HOMO−1 are shown in Figure 1 along with a Lewis representation of **1**

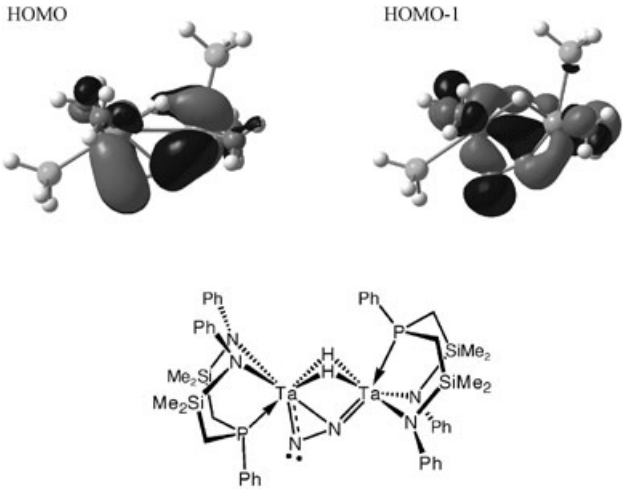

Figure 1. Depictions of the HOMO and HOMO−1 calculated for a model complex of **1**, and a simple Lewis dot structure that shows both a Ta–N π bond (dashed) and a lone pair on the terminal N atom.

that summarizes their contributions to bonding. The HOMO (left) is dominated by π-interactions between d orbitals on each Ta and the π_v^* (v = vertical) orbital of the dinitrogen unit. We propose that this molecular orbital allows for the addition of simple hydride reagents, such as alkyl boron hydrides and silanes, across the Ta–N unit resulting in a terminal tantalum hydride and a functionalized nitrogen atom. HOMO−1 (right) arises from interactions between d orbitals on Ta and the π_h^* (h = horizontal) orbital of the dinitrogen unit. The isosurface calculated for HOMO−1 shows a lobe of electron density on the exposed nitrogen atom of the N_2 unit that can be anticipated to act in a σ-donor fashion with Lewis acids.

Herein we describe the synthesis, structure, and vibrational spectroscopic properties of Lewis acid adducts of **1** with trimethylgallium (**2**), trimethylaluminum (**3**), and tris(pentafluorophenyl)boron (**4**) [Eq. (2)]. The N–N distance is elongated in these complexes relative to that in **1**; this suggests an additional activation of the N_2 unit by the Lewis acids. As before, vibrational data are evaluated by normal coordinate analysis (NCA) which employs a force field generated by DFT.[15] On the basis of the DFT calculation, the electronic structure of the Lewis adducts is described and compared to that of complex **1**. The implications of these results are discussed with respect to the ability of Lewis acids to further activate the coordinated N_2 molecule, ultimately leading to N–N bond cleavage.

Results

Synthesis and molecular structure

*Synthesis, molecular structure, and solution behavior of [{(NPN)Ta}$_2$(μ-H)$_2$(μ-η^1:η^2-NNAlMe$_3$)] (**3**)*: Previously, the equilibrium constant between end-on mononuclear dinitrogen complexes and $AlMe_3$ adducts in the presence of $AlMe_3$ was used to compare and quantify the σ-donor strengths of end-on mononuclear N_2 complexes.[17,18] The reaction between **1** and $AlMe_3$ to give [{(NPN)Ta}$_2$(μ-H)$_2$(μ-η^1:η^2-NNAlMe$_3$)] (**3**) proceeds almost instantly as indicated by a rapid color change during mixing. No equilibrium between **1** and **3** is observed, and a solution of labeled [$^{15}N_2$]-**1** and unlabeled **3** shows no formation of [$^{15}N_2$]-**3**. These data suggest the formation of **3** is irreversible. The solid-state molecular structure of **3** was determined by X-ray crystallography, and is shown in Figure 2. The Al atom is clearly four-coordinate and trigonal pyramidal. The bridging hydrides were not located, but are strongly implied by a doublet of doublets (J_{HP} = 20.3 and 14.3 Hz) at δ = 10.85 ppm integrating to two protons in the ^{1}H NMR spectrum. Metric parameters of the Ta_2N_2 moiety of **3** are similar to those of **1** (Table 1), with the N5–N6 distance increasing by 0.036 Å to 1.363(7) Å in **3**.

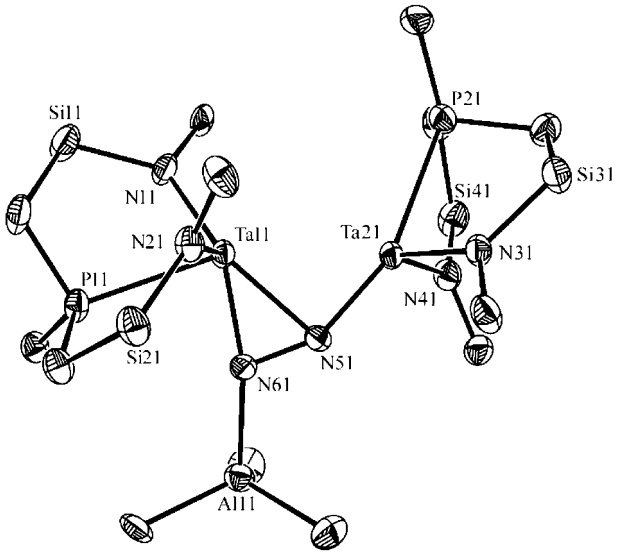

Figure 2. ORTEP drawing (spheroids at 50% probability) of **3**. Only one of two independent molecules in the asymmetric unit is shown. Silylmethyl and phenyl ring carbon atoms other than ipso omitted for clarity. Selected bond lengths [Å] and angles [°]: N5–N6 1.363(7), Ta1–N5 2.138(5), Ta1–N6 1.961(5), Ta2–N5 1.873(5), N6–Al1 1.993(5), Ta2-N5-N6 150.6, Al1-N6-Ta1 166.1(3), N5-N6-Al1 114.7(4).

Table 1. Labeling scheme and selected bond lengths [Å] and angles [°] for compounds **2**, **3**, and **4**.

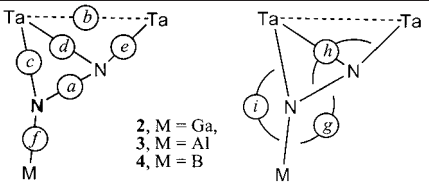

	2	**3**	**4**
a	1.356(18)	1.363(7)	1.393(7)
b	2.8560(9)	2.850(2)	2.9198(3)
c	1.960(12)	1.961(5)	2.002(5)
d	2.149(14)	2.138(5)	2.155(5)
e	1.909(12)	1.873(5)	1.904(5)
f	2.101(12)	1.993(5)	1.584(9)
g	111.8(9)	114.7(4)	116.6(5)
h	148.1(11)	150.6(3)	151.3(4)
i	169.1(7)	166.1(3)	166.1(4)

A broadening of some ^{1}H NMR resonances associated with a fluxional process occurs near room temperature for **3**. In the high-temperature limit, this complex appears to have C_s symmetry, whereas when the sample is cooled to 240 K, it appears to have C_1 symmetry (reminiscent of the solid-state structure), based on the number and integrations of the silylmethyl resonances. Free rotation occurs about the N–Al bond in both cases, because only one aluminum–methyl resonance is observed in the ^{1}H NMR spectrum even at 240 K. A fluxional process involving the rocking of the NPN ligand fragments, such that the P-Ta-Ta-P dihedral angle passes through 180° may be responsible for the apparent C_s symmetry at room temperature; a similar process is also observed for **1** at much lower temperatures. It is likely that the temperature difference results from hindered movement of the ancillary ligands due to the presence of the $AlMe_3$ moiety.

The [^{15}N]-labeled analogue [$^{15}N_2$]-**3** was prepared in an identical manner using the 99% isotopically enriched precursor [{(NPN)Ta}$_2$(μ-H)$_2$(μ-η^1:η^{2}-[$^{15}N_2$])] ([$^{15}N_2$]-**1**). The ^{15}N{^{1}H} NMR spectrum of [$^{15}N_2$]-**3** is composed of two resonances; a resonance at δ = −33.1 ppm is strongly coupled to one ^{31}P nucleus with a $^2J_{NP}$ value of 25 Hz and is also coupled to the adjacent ^{15}N nucleus with a $^1J_{NN}$ value of 18.8 Hz. The chemical shift of this resonance is consistent with its assignment as the bridging N atom (N5 in Figure 2) of the dinitrogen moiety. The second ^{15}N resonance, assigned as the terminal Al-bound N atom (N6 in Figure 2), occurs at δ = 54.6 ppm and is coupled to a ^{31}P nucleus with a $^2J_{NP}$ value of 8.4 Hz as well as the adjacent ^{15}N nucleus. The chemical shift of the terminal N atom is clearly affected by the involvement of its lone pair in a dative bond to Al ([$^{15}N_2$]-**1** shows resonances for $N_{bridging}$ at δ = −20.4 ppm and $N_{terminal}$ at 163.6 ppm). The ^{31}P{^{1}H} NMR spectrum of [$^{15}N_2$]-**3** reveals that additional couplings between ^{31}P and ^{15}N are present, with $^2J_{PN}$ and $^3J_{PN}$ values of 2.8 and 2.0 Hz respectively. These couplings could not be adequately resolved in the ^{15}N{^{1}H} NMR spectrum.

*Synthesis, molecular structure, and solution behavior of [{(NPN)Ta}$_2$(μ-H)$_2$(μ-η^1:η^2-NNGaMe$_3$)] (**2**)*: The 1:1 reaction of **1** and $GaMe_3$ quantitatively produces [{(NPN)Ta}$_2$(μ-

H)$_2$(μ-η^1:η^2-NNGaMe$_3$)] (**2**). The solid-state molecular structure of **2** has been established by X-ray diffraction of a twinned crystal, and, as for **3**, there are two distinct but chemically identical molecules within the asymmetric unit. An ORTEP drawing of one of these molecules is shown in Figure 3; metric parameters are given in Table 1.

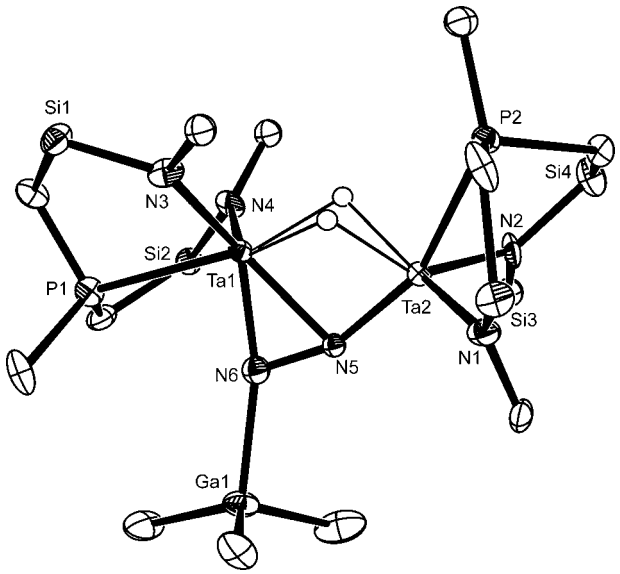

Figure 3. ORTEP drawing (spheroids at 50% probability) of **2**. Only one of two independent molecules in the asymmetric unit is shown. Silylmethyl and phenyl ring carbon atoms other than ipso omitted for clarity. Selected bond lengths [Å] and angles [°]: N5–N6 1.356(18), Ta1–N5 2.149(14), Ta1–N6 1.960(12), Ta2–N5 1.909(12), N6–Ga1 2.101(12), Ta1–Ta2 2.8560(9), Ta2-N5-N6 148.1(11), Ga1-N6-Ta1 169.1(7), N5-N6-Ga1 111.8(9). Hydrides were modeled with X-HYDEX. (A. G. Orpen, *J. Chem. Soc. Dalton Trans.*, **1980**, 2509.)

Both this molecular structure and the ^{1}H and ^{31}P{^{1}H} NMR spectra of **2** are extremely similar to those of **3**, as expected. The N6–Ga1 bond is longer than the N6–Al1 bond in **3** by 0.108 Å, which is slightly greater than the difference in the covalent radii of Al and Ga, but very similar to the difference reported between Al and Ga adducts of the nitrogenous base 5,6-benzoquinoline.[19] In solution, complex **2** displays fluxional processes analogous to those reported for **3** above; however, the low-temperature limiting spectrum is evident at room temperature and only above 320 K does the interconversion process become fast enough on the NMR timescale to generate C_s symmetry. The ^{15}N{^{1}H} NMR spectrum of labeled analogue [^{15}N$_2$]-**2** is quite similar to that of [^{15}N$_2$]-**3**, with resonances at $\delta = -29.9$ and 79.9 ppm coupled by $^1J_{NN} = 18.3$ Hz.

*Synthesis, molecular structure, and solution behavior of [{(NPN)Ta}$_2$(μ-H)$_2${μ-η^1:η^2-NNB(C$_6$F$_5$)$_3$}] (**4**)*: Attempts to prepare an isolable trialkylboron adduct of **1** either from BMe_3 or from BEt_3 were unsuccessful, leading to a number of products as observed by ^{31}P{^{1}H} NMR spectroscopy. None of these products had NMR resonances reminiscent of **2** or **3**. However, the Lewis acid B(C$_6$F$_5$)$_3$ forms an adduct with **1** despite the considerable steric bulk imposed by the three perfluorophenyl groups, demonstrating the accessibility of the terminal nitrogen of **1** to other reagents. The reaction proceeds immediately at room temperature as monitored by ^{31}P{^{1}H} NMR spectroscopy to give [{(NPN)Ta}$_2$(μ-H)$_2${μ-η^1:η^2-NNB(C$_6$F$_5$)$_3$}] (**4**). This complex gives resonances in the ^{31}P{^{1}H} NMR spectrum at $\delta = 11.6$ and 17.7 ppm coupled to each other by $J_{PP} = 23.9$ Hz. Over the course of 48 h, complex **4** crystallizes from solution; the solid-state molecular structure of **4** as determined by X-ray crystallography is shown in Figure 4. The bond lengths and angles of the dinitrogen moiety in **4** are again very similar to those found in complex **1** (Table 1). There are a number of donor adducts of B(C$_6$F$_5$)$_3$ that have been structurally characterized,[20–25] although none have been reported previously in dinitrogen coordination chemistry.

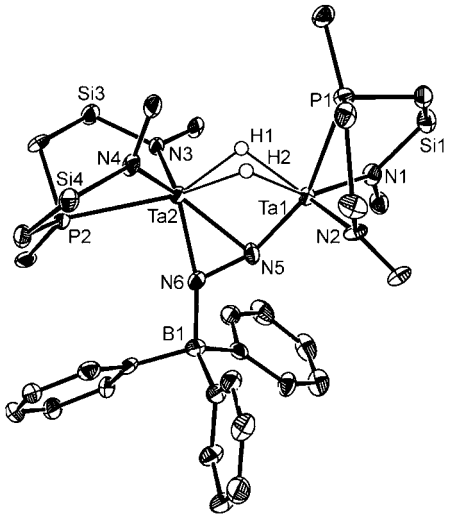

Figure 4. ORTEP drawing (spheroids at 50% probability) of **4**. Silylmethyl and ligand phenyl ring carbon atoms other than ipso and all fluorine atoms omitted for clarity. Selected bond lengths [Å] and angles [°]: N5–N6 1.393(7), Ta1–N5 1.904(5), Ta2–N5 2.155(5), Ta2–N6 2.002(5) N6–B1 1.584(9), Ta1–Ta2 2.9198(3), Ta1–P1 2.651(2), Ta2–P2 2.713(2), Ta1–N1 2.049(5), Ta1-N5-N6 151.3(4), B1-N6-Ta2 166.1(4), N5-N6-B1 116.6(5), Ta2-N6-N5 76.5(3). Hydride ligands were located in the difference map and refined isotropically.

The [^{15}N$_2$]-labeled analogue of **4** has two resonances in its ^{15}N{^{1}H} NMR spectrum. The peak at $\delta = -21.2$ is coupled to one ^{31}P nucleus with a $^2J_{NP}$ value of 22.0 Hz, and is also coupled to the adjacent ^{15}N with a $^1J_{NN}$ value of 15.3 Hz. This can be assigned as $N_{bridging}$ (N5 in Figure 4), due to the similarity in chemical shift to that reported for complex [^{15}N$_2$]-**1** ($\delta = -20.4$ ppm). The ^{31}P coupling is presumably due to the *trans*-disposed ^{31}P nucleus. The other ^{15}N resonance appears at $\delta = 2.4$ ppm as a doublet, with a $^1J_{NN}$ value of 15.3 Hz. A fluxional process similar to that already described for **1**, **2**, and **3** is operant, with the high-temperature-limiting C_s symmetry being observed well above room temperature at 340 K.

Vibrational spectroscopic analysis: The basic vibrational structure of the adducts [{(NPN)Ta}$_2$(μ-H)$_2$(μ-η^1:η^2-N$_2$-GaMe$_3$)] (**2**), [{(NPN)Ta}$_2$(μ-H)$_2$(μ-η^1:η^2-N$_2$-AlMe$_3$)] (**3**), and [{(NPN)Ta}$_2$(μ-H)$_2${μ-η^1:η^2-N$_2$-B(C$_6$F$_5$)$_3$}] (**4**) is found to be analogous to that of the parent complex [{(NPN)Ta}$_2$(μ-H)$_2$(μ-η^1:η^2-N$_2$)] (**1**). Eigenvectors of the vibrations of **2** and **4** resulting after normal coordinate analysis (see below) are given in Figures 5 and 6, respectively. As in the case of **1**, four in-plane and two out-of-plane normal modes of the Ta$_2$(μ-η^1:η^2-N$_2$) core can be identified. These vibrations are assigned to the N–N stretch, one Ta2-η^1-N$_2$ mode, two Ta1-η^2-N$_2$ modes (symmetric and asymmetric), and two out-of-plane modes (symmetric and asymmetric) of the dinitrogen unit. Detailed spectroscopic studies on **1** have lead to the identification of five from these six vibrations, the symmetric out-of-plane mode not having been observable.

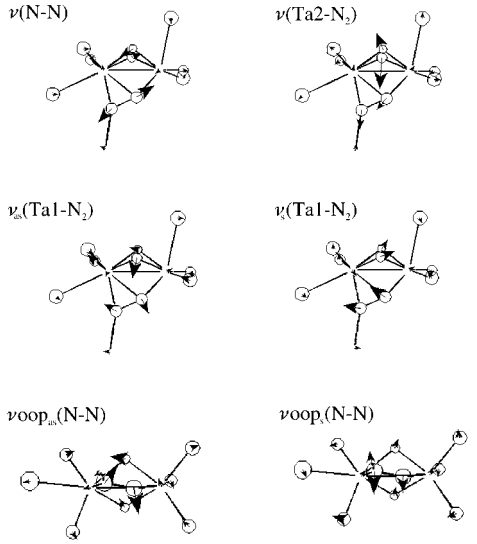

Figure 5. Eigenvectors of the six modes of the Ta$_2$N$_2$ unit of **II**. The arrows correspond to unit displacements with a scaling factor of 2.

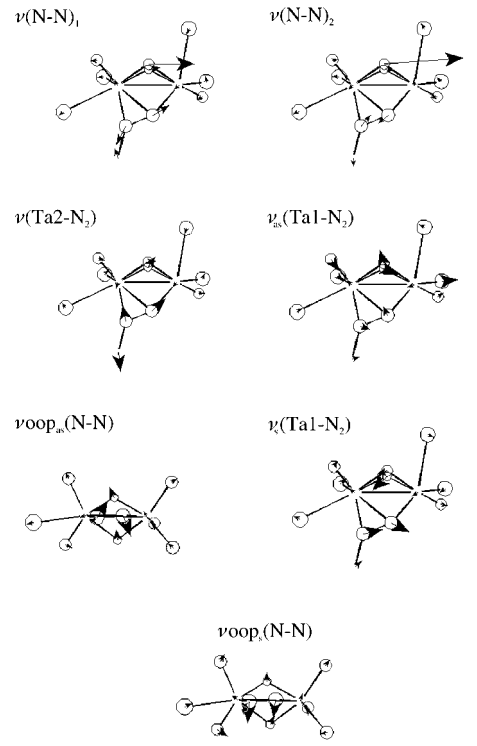

Figure 6. Eigenvectors of the six modes of the Ta$_2$N$_2$ unit of **IVa**. The arrows correspond to unit displacements with a scaling factor of 2.

Solid-state resonance Raman spectra of **2**, **3**, and **4** and their ^{15}N-labeled derivatives are shown in Figure 7. The spectra were recorded at an excitation wavelength of 568.2 nm, which provides strong resonance enhancement to the vibrations of the Ta$_2$(μ-η^1:η^2-N$_2$) core. Vibrational frequencies are collected and compared to those found for complex **1** in Table 2. The N–N stretching frequency of **1** was found at 1165 cm^{-1} with a ^{15}N isotope shift of −37 cm^{-1}. In the Raman spectra of adducts **2** and **3** this vibration appears at 1128 cm^{-1} (**2**) and 1131 cm^{-1} (**3**), exhibiting ^{15}N isotope shifts of −32 and −33 cm^{-1}, respectively. The Raman spectrum of complex **4** displays a broad peak for ν(N–N) at 1154 cm^{-1}, shifting to 1119 cm^{-1} upon substitution with ^{15}N; both features are strongly decreased in their intensity with respect to **2** and **3**. Thus, all N–N stretching modes of the derivatives are lowered in energy relative to **1**, in agreement with the observed lengthening of the N–N bond upon adduct formation.

In the metal–ligand stretching vibration region further peaks exhibiting isotope shifts appear. The end-on Ta-N$_2$ mode ν(Ta2-N$_2$) of **1** was found at 656 cm^{-1} ($^{15}\Delta$ = −16 cm^{-1}), showing slight mixing with a vibration at 668 ($^{15}\Delta$ = −4 cm^{-1}), which was attributed to a metal–terminal-ligand NPN stretch. In the Lewis adducts **2**–**4**, ν(Ta2-N$_2$) shifts to *higher* energy, which increases its mixing with terminal ligand modes, thus distributing this vibration over a cluster of peaks. Thus in the case of **2** there are isotope sensitive modes at 749, 739, 727, 709, and 698 cm^{-1}. The same applies to **3** for which three modes at 758, 742, and 730 cm^{-1} are found ($^{15}\Delta$ = −10, −4, and −13 cm^{-1}). The cumulative isotope shift of these features (−25 cm^{-1} in **2** and −27 cm^{-1} in **3**) approximately corresponds to the isotope shift observed for ν(Ta2-N$_2$) in complex **1**. In the spectra of complex **4** ν(Ta2-N$_2$) appears at even higher energy, splitting into three peaks at 926, 828, and 778 cm^{-1} ($^{15}\Delta$ = −5, −8, and −5 cm^{-1}).

As described before, symmetric and asymmetric vibrations are found for the side-on bonding of N$_2$ to Ta1. The position of the *asymmetric* mode ν_{as}(Ta1-N$_2$) does not change significantly in the spectra of **2**, **3**, and **4** with respect to **1**; that is, this mode is located at about 630 cm^{-1} in all spectra. Raman resonance enhancement of this vibration, however, is found to be much smaller for the Lewis adducts **2**, **3**, and **4** than for **1**. The same applies to the ^{15}N isotope shifts, which are markedly reduced for **2** and **3** relative to **1** (−14 and −12 cm^{-1} vs −22 cm^{-1}, respectively). In the Raman spectra of **4** an additional isotope sensitive feature appears at 568 cm^{-1} ($^{15}\Delta$ = −9 cm^{-1}), which can be attributed to mixing of ν_{as}(Ta1-N$_2$) with a metal-terminal ligand mode.

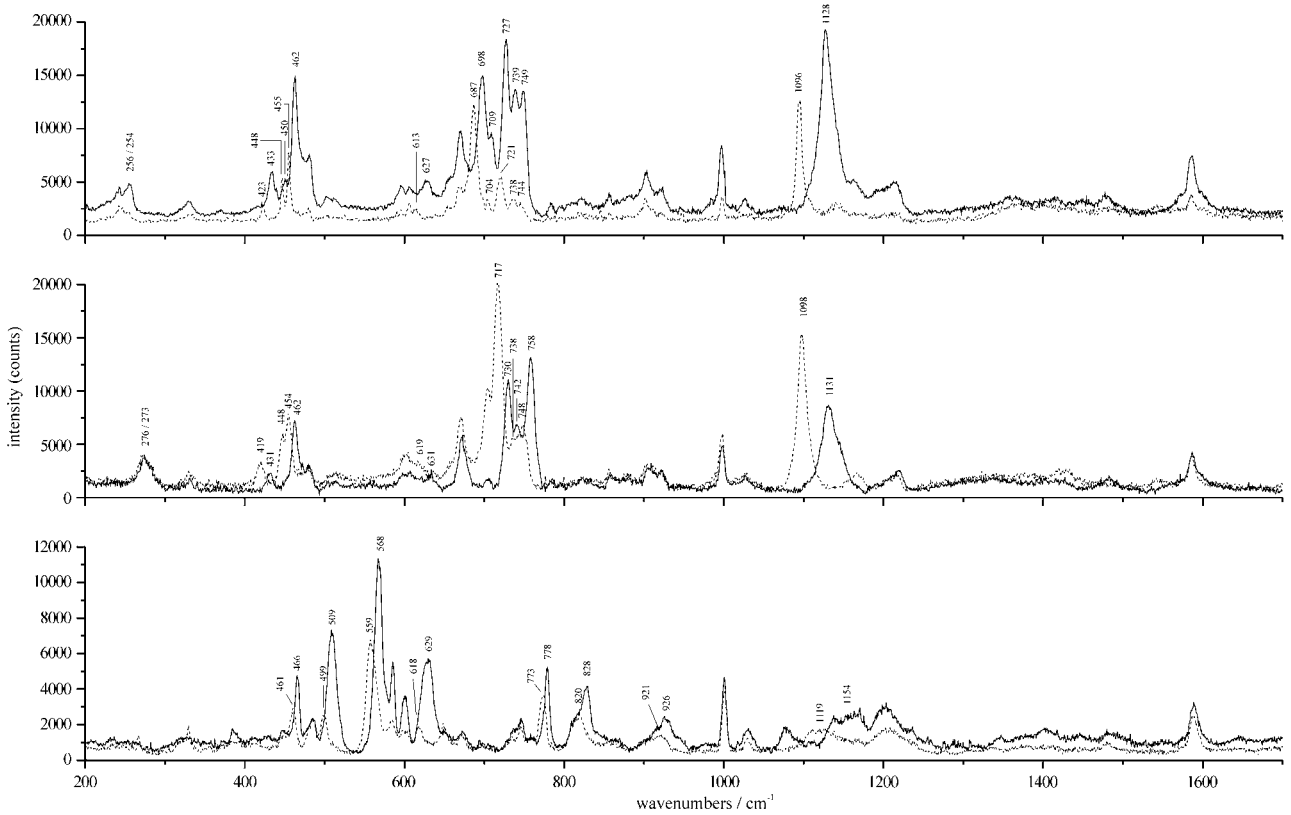

Figure 7. Raman spectra of **2** (top), **3** (middle), and **4** (bottom) recorded with an excitation wavelength of 568.2 nm at 10 K. Solid line: natural abundance; dashed line [$^{15}N_2$]-labeled derivative.

Table 2. Comparison and assignments of the observed frequencies of complexes **2**–**4** with those found for complex **1**.

	1[b]		**2**		**3**		**4**	
	^{14}N	^{15}N	^{14}N	^{15}N	^{14}N	^{15}N	^{14}N	^{15}N
ν(N-N)	1165	1128	1128	1096	1131	1098	1154	1119
	1165[a]	1128[a]	1131[a]	1095[a]	1132[a]	1098[a]	1145[a]	1119[a]
ν(Ta2-N_2)	656	643	749	744	758	748	926	921
		636	739	738	742	738	828	820
			727	721	730	717	778	773
			709	704				
			698	687				
ν_{as}(Ta1-N_2)	625	603	627	613	631	619	629	618
	625[a]	604[a]	628[a]	621[a]	630[a]	621[a]	568	559
							700[a]	698[a]
							673[a]	670[a]
							649[a]	647[a]
							633[a]	630[a]
							621[a]	616[a]
							570[a]	568[a]
ν_s(Ta1-N_2)	487	482	462	455	462	454	466	461
	487[a]	482[a]	463[a]	456[a]	462[a]	448	437[a]	429[a]
	469	463	450	448	451[a]	454[a]		
	469[a]	465[a]	451[a]	447[a]		447[a]		
νoop$_{as}$(N-N)	442	432	433	423	431	419	509	499
νoop$_s$(N-N)	n.o.	n.o.	256	254	276	273	409[a]	404[a]
			256[a]	254[a]	276[a]	273[a]		

[a] IR data; unlabeled data is Raman data; n.o. = not observed. [b] Data taken from reference [15].

The *symmetric* component of the Ta1-N_2 vibration is lowered in energy for **2**, **3** and **4** by about 20 cm^{-1} relative to **1**, being located at 462 cm^{-1} in **2** and **3** and at 466 cm^{-1} in **4**. In the spectra of **2** this feature shifts to 455 cm^{-1} upon isotope substitution. Another peak at 450 cm^{-1} also displays slight isotope sensitivity ($^{15}\Delta = -2$ cm^{-1}), such that summation of these two shifts leads to an overall isotope shift of -9 cm^{-1} for ν_s(Ta1-N_2) in **2**. In the spectra of complex **3**, the ν_s(Ta1-N_2) mode shifts from 462 cm^{-1} to 454 cm^{-1}. There is an additional peak in the Raman spectrum of the ^{15}N-labeled derivative located at 448 cm^{-1}. Its counterpart is not found in the Raman spectrum of unlabeled **3**, but, instead, is observed in the IR spectrum at 451 cm^{-1} (see below). Taking the two shifts together gives an isotope shift

of $-11\,cm^{-1}$. In the spectra of **4**, finally, ν_s(Ta1-N_2) is observed at 466 cm^{-1}, exhibiting a ^{15}N isotope shift of $-5\,cm^{-1}$. IR spectroscopy evidences a second component of this vibration, too (vide infra).

The symmetric out-of-plane mode γoop_s(N-N), which was not observed in complex **1**, is found in the Raman spectra of complex **2** at 256 cm^{-1} ($^{15}\Delta = -2\,cm^{-1}$) and in complex **3** at 276 cm^{-1} ($^{15}\Delta = -3\,cm^{-1}$); in the Raman spectrum of complex **4** it is not observed. The energy of the asymmetric out-of-plane mode of the Ta_2N_2 moiety γoop_{as}(N-N) decreases by about 10 cm^{-1} in **2** (433 cm^{-1}, $^{15}\Delta = -10\,cm^{-1}$) and **3** (431 cm^{-1}, $^{15}\Delta = -12\,cm^{-1}$) with respect to **1** (442 cm^{-1}, $^{15}\Delta = -10\,cm^{-1}$). In contrast, the frequency of this mode is increased for **4** by 45 cm^{-1} (509 cm^{-1}, $^{15}\Delta = -10\,cm^{-1}$) relative to **1**.

Additional information on the vibrational properties of complexes **2**–**4** can be inferred from infrared spectroscopy (Figure 8, Table 2). Here the N–N stretching band is found at 1131 ($^{15}\Delta = -36\,cm^{-1}$; **2**), 1132 ($^{15}\Delta = -34\,cm^{-1}$; **3**) and 1145 cm^{-1} ($^{15}\Delta = -26\,cm^{-1}$, **4**), in agreement with the Raman data (Table 2). The end-on Ta-N2 mode ν(Ta2-N_2) is not observed, whereas the asymmetric side-on vibration ν_{as}(Ta1-N_2) is found at 628 (**2**; $^{15}\Delta = -7\,cm^{-1}$) and 630 cm^{-1} (**3**; $^{15}\Delta = 9\,cm^{-1}$), respectively. In the spectra of complex **4** this mode is distributed over several bands at 700, 673, 649, 633, 621, and 570 cm^{-1} all of which exhibit small isotope shifts upon substitution with ^{15}N. This qualitatively agrees with the findings for ν_{as}(Ta1-N_2) in the Raman spectra of **4** (vide supra). In further analogy to the Raman data, the symmetric mode ν_s(Ta1-N_2) is split into two bands at 463 ($^{15}\Delta = -7\,cm^{-1}$)/ 451 cm^{-1} ($^{15}\Delta = -4\,cm^{-1}$) for **2** and 462 ($^{15}\Delta = -8\,cm^{-1}$)/ 451 cm^{-1} ($^{15}\Delta = -4\,cm^{-1}$) for **3**. This mode is also split into two vibrations in the spectra of **4** (466 and 437 cm^{-1}), but in contrast to the spectra of **2** and **3**, the 466 cm^{-1} feature is only observed in the Raman (see above) spectrum, whereas the feature at 437 cm^{-1} only appears in the IR spectrum. The overall ^{15}N isotope shift of this mode thus amounts to $-13\,cm^{-1}$. Finally, the symmetric out-of-plane mode νoop_s(N-N) can be identified in the infrared spectra of **2** and **3** at 256 and 276 cm^{-1}, with isotope shifts of -2 and $-3\,cm^{-1}$, respectively. In the spectrum of complex **4** there is an isotope sensitive band at 409 cm^{-1} ($^{15}\Delta = -5\,cm^{-1}$) that can be attributed to νoop_s(N-N). However, the large upshift of this mode with respect to **2** and **3** is not accounted for by the DFT frequency calculation.

Of further interest are the vibrations of the coordinated Lewis acid. While the totally symmetric stretching mode ν(X-R_3) (R = Me in **2** and **3** and C_6F_5 in **4**) cannot be identified in the Raman spectra of complexes **2**–**4**, it is calculated by DFT at 496 and 507 cm^{-1} for models **II** and **III**, respectively (the structures of these models are depicted in the next section). The nitrogen/Lewis acid stretching vibration ν(N-X) is not observed either, being calculated for model **III** ($AlMe_3$ adduct) at 260 cm^{-1}. Due to the lower N–X

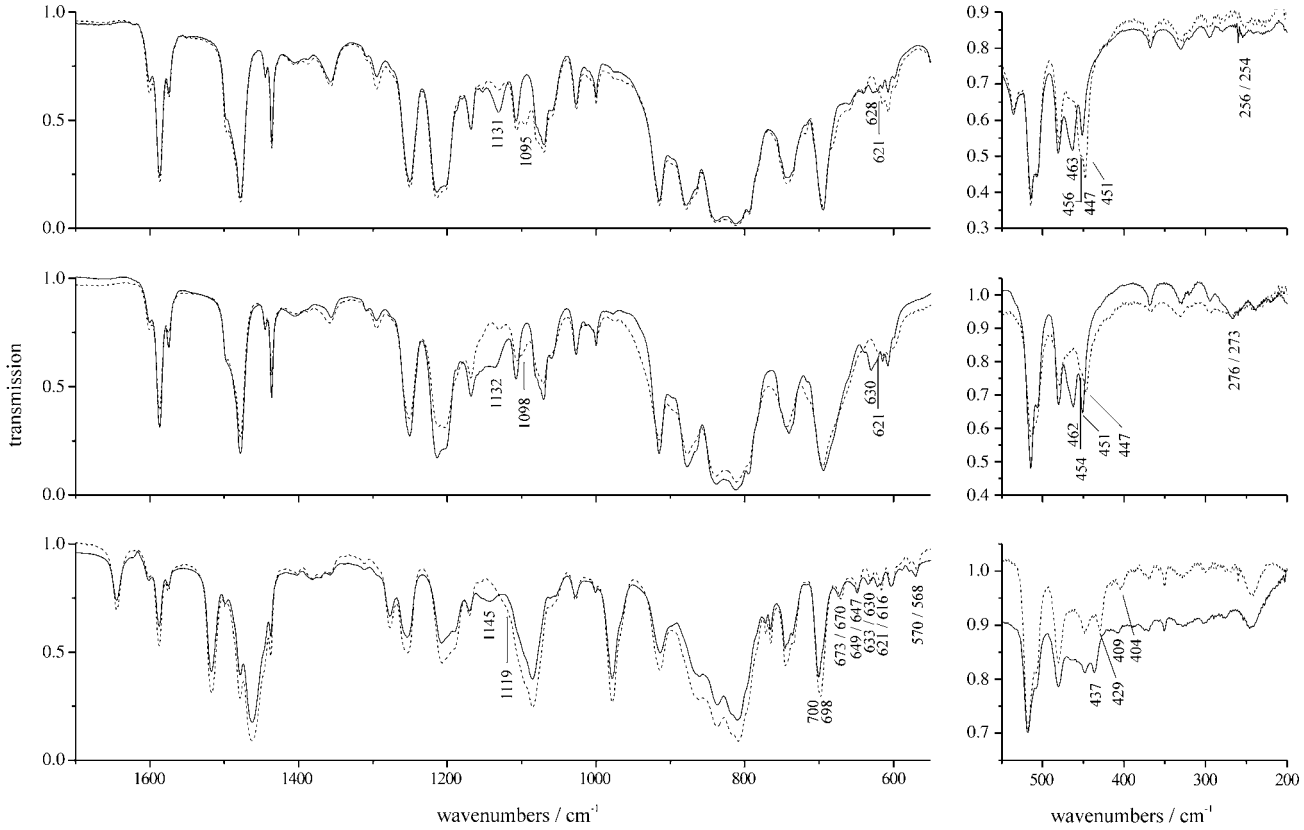

Figure 8. IR spectra of **2** (top), **3** (middle), and **4** (bottom). Solid line: natural abundance; dashed line [$^{15}N_2$]-labeled derivative.

bond order and the higher mass of the Lewis acid in **II** ($GaMe_3$ adduct), ν(N-X) should shift to lower energy in this adduct. However, this mode cannot be identified in the frequency calculation for model **II** due to severe mixing with other vibrations. DFT frequency calculations for model complex **IVb** result in a distribution of ν(X-R_3) and ν(N-X) over several modes at approximately 1050 and 900 cm^{-1}, respectively.

Quantum-chemistry-based normal coordinate analysis (QCB-NCA): The vibrational data of complexes **2–4** were converted into a set of force constants by employing the QCB-NCA procedure (quantum-chemistry-based normal coordinate analysis), which was developed earlier to account for the vibrational properties of complex **1**. The calculation of theoretical force fields for compounds **2–4** is based on models **II**, **III**, and **IVa**. These structures are simplified by replacing the NPN ligands by NH_2 and PH_3 groups. In case of complex **4**, the $B(C_6F_5)_3$ group is replaced by BH_3. In the course of the QCB-NCA procedure the hydrogen atoms of the NH_2 and PH_3 groups are removed to avoid artificial interactions. Additionally the masses of the boron hydrogen atoms in model **IVa** are set to 167, the mass of the C_6F_5 groups, to approximate the $B(C_6F_5)_3$ group. In addition to the five internal coordinates of model **I** (r_{NN}, $r_{TaN}1$–$r_{TaN}3$ and γ_{NN}), the force constant of the N–X bond (r_{NX}) (X = Ga, Al or B) is taken into account. The force constants of the metal–ligand bonds to the terminal N and P donor atoms as well as to the bridging hydrido ligands are fixed at their theoretical values derived from the DFT calculations. Apart from a few off-diagonal elements of the Ta_2N_2 unit, designated a–f, all other off-diagonal elements in the submatrix of the Ta_2N_2 unit are fixed at their calculated DFT values. The resulting f-matrix is shown in Scheme 1. Finally, 11 force constants of each model complex **II**, **III**, and **IVa** are fitted to match the observed frequencies.

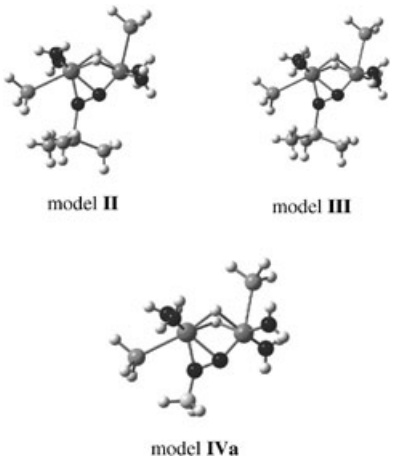

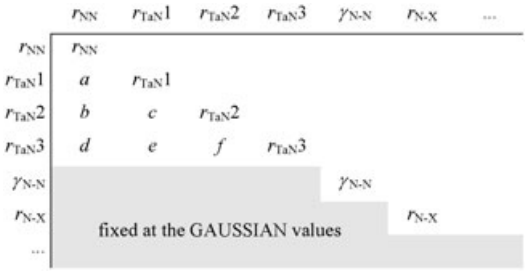

Scheme 1. f-Matrix.

The experimentally determined frequencies are compared to the values derived from QCB-NCA in Table 3. Overall agreement is quite good, apart from the following discrepancies: The N–N stretch in model **IVa** is split into two features that show strong mixing with metal–hydrido modes; this is not observed. Furthermore, ν(Ta2-N_2) is calculated to well-defined, single frequencies for **II**, **III**, and **IVa**, whereas this vibration is distributed over several features in the measured spectra of compounds **2**, **3**, and **4** as a result of mixing with metal–terminal-ligand modes (vide supra). However, the overall isotope shift obtained experimentally fits to the theoretically calculated value. In contrast, the ν_{as}(Ta1-N_2) mode is observed as a single feature in the spectra of complexes **2**

Table 3. Comparison of the observed frequencies for complexes **2–4** with the QCB-NCA results of models **II**, **III**, and **IVa**.

mode	**2**				**3**				**4**			
	exptl		QCB-NCA		exptl		QCB-NCA		exptl		QCB-NCA	
	^{14}N	^{15}N	^{14}N	^{15}N	^{14}N	^{15}N	^{14}N	^{15}N	^{14}N	^{15}N	^{14}N	^{15}N
ν(N-N)	1128	1096	1131	1095	1131	1098	1133	1096	1154	1119	1170	1160
											1151	1124
ν(Ta2-N_2)	749	744	740	718	758	748	744	721	926	921	883	865
	739	738			742	738			828	820		
	727	721			730	717			778	773		
	709	704										
	698	687										
ν_{as}(Ta1-N_2)	627	613	645	642	631	619	647	644	629	618	598	586
			636	629			638	631	568	559	657	651
			621	618			628	626			615	611
			617	612			621	615				
ν_s(Ta1-N_2)	462	455	463	450	462	454	462	449	466	461	464	450
	450	448				448						
νoop_{as}(N-N)	433	423	435	421	431	419	431	419	509	499	509	493
νoop_s(N-N)	256	254	269	264	276	273	279	275	409	404	309	301

and **3** (in compound **4** this mode is split into two bands), whereas this mode is distributed over several modes in the QCB-NCA fit. This indicates that the terminal ligand modes are at lower frequency in the calculation than observed in the experiment.

The force fields obtained for the Ta_2N_2 unit of the three different complexes **2**–**4** are given in Table 4 and compared to those found for the parent complex **1**. As expected by

Table 4. Force constants of the internal coordinates of the Ta_2N_2 unit of complexes **I**, **II**, **III**, and **IVa**.

	Force constant[a]			
	I[b]	**II**	**III**	**IVa**
r_{NN}	2.430	1.876	1.729	1.515
$r_{TaN}1$	1.291	1.233	1.194	1.105
$r_{TaN}2$	0.917	0.800	0.836	1.090
$r_{TaN}3$[c]	2.517	2.880	2.860	2.486
γ_{NN}	0.482	0.557	0.448	1.055
r_{NX}		1.032	1.389	2.601
a	0.576	0.262	0.301	0.559
b	0.586	0.676	0.773	0.481
c	0.651	0.837	0.872	0.953
d	0.292	0.421	0.465	0.012
e	0.038	0.025	−0.135	0.364
f	0.122	0.238	0.255	0.388

[a] Units are mdyn Å^{-1}. [b] Data taken from reference [15]. [c] Side-on Ta–N.

consideration of N–N bond lengths (1.356 (**2**), 1.363 (**3**) and 1.393 Å (**4**)), the force constants of the N–N bonds decrease in the Lewis acid adducts **2**–**4** relative to the parent complex **1** (N–N bond length 1.32 Å). In agreement with the sequence of N–N bond lengths, the N–N force constants decrease from 2.430 mdyn Å^{-1} (**1**)[15] to 1.876 (**2**), 1.729 (**3**) and 1.515 mdyn Å^{-1} (**4**). In contrast, the metal–nitrogen force constants $r_{TaN}1$–$r_{TaN}3$ are in the same range for all complexes **1**–**4**. The force constant for the out-of-plane mode γ_{NN} in complexes **2** and **3** are similar to that found in complex **1** (0.482 mdyn Å^{-1}), but strongly increases in compound **4** to a value of 1.055 mdyn Å^{-1}. Finally, the force constants for the N–X bonds (X = Ga, Al and B) are 1.032, 1.389 and 2.601 mdyn Å^{-1}.

Electronic structure: The electronic structures of **2**–**4** are discussed based on model complex **IVa**, $[\{PH_3(NH_2)_2Ta\}_2(\mu\text{-}H)_2(\mu\text{-}\eta^1{:}\eta^2\text{-}N_2\text{-}BH_3]$, which was employed for the vibrational analysis of the tris(pentafluorophenyl)boron adduct **4** (vide supra). Here **IVa** serves as a generic model of the three Lewis adducts **2**, **3**, and **4**. Similar calculations have been performed for model **I** which is $[\{PH_3(NH_2)_2Ta\}_2(\mu\text{-}H)_2(\mu\text{-}\eta^1{:}\eta^2\text{-}N_2)]$.[15] Figure 9 shows a section of the molecular orbital diagram of **IVa**; contour plots and charge contributions of important molecular orbitals are given in Figure 10 and Table 5, respectively. The model is oriented such that the *x* axis is along the Ta–Ta vector and the *y* axis lies within the Ta_2N_2 plane. The π_v and π_v^* orbitals of the dinitrogen ligand are vertical (v) to this plane, whereas the π_h and π_h^* orbitals lie in this plane (horizontal, h; cf. Figure 1).

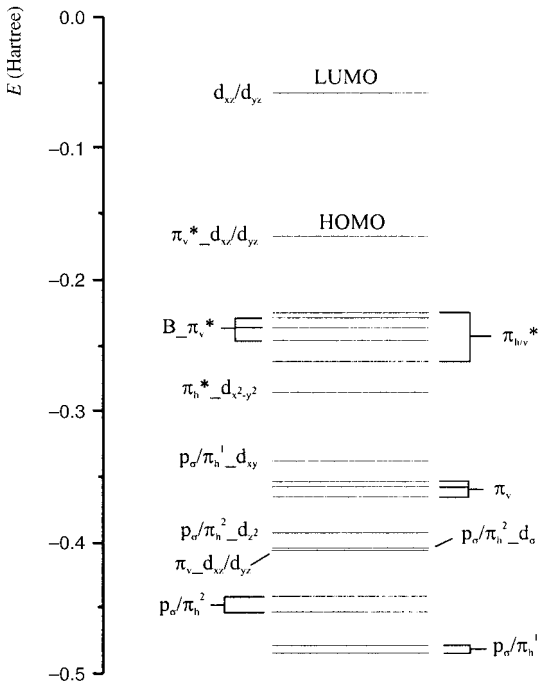

Figure 9. MO diagram of model **IVa**. MO designations correspond to those in Table 5.

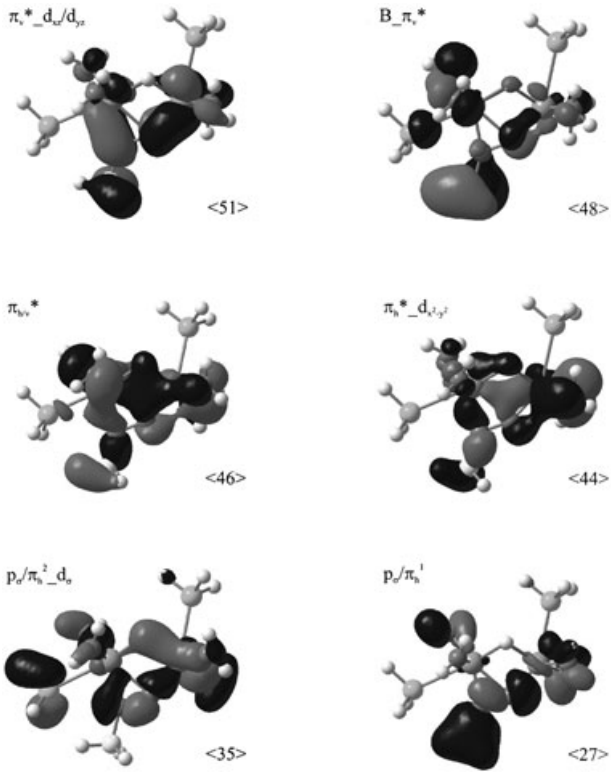

Figure 10. Contour plots of important molecular orbitals of **IVa**.

The HOMO of **IVa**, $\pi_v^*\_d_{xz}/d_{yz}$ ⟨51⟩, has dominant nitrogen character and derives from a bonding combination of the π_v^* function of the dinitrogen unit with the mixed d_{xz}/d_{yz}

Table 5. Charge contributions of model **IVa**.[a]

Orbital	Label	Energy [Hartree]	Charge Decomposition [%] Ta1 d	Ta2 d	N_t[b]	N_b[b]	$(\mu\text{-H})_2$[c]	N_{AD}[c,d]	PH_3[c]	B	remark[e]
d_{xz}/d_{yz}	52	−0.05931	24	33	1	2	0	5	13	1	LUMO
π^*_{v}–d_{xz}/d_{yz}	51	−0.16803	12	20	28	10	1	9	1	5	HOMO π a.b.
$\pi^*_{h/v}$	50	−0.22533	4	1	6	11	2	56	9	5	π b.
B	49	-0.22959	2	1	6	4	1	14	2	35	n.b.
B–π^*_{v}	48	−0.23824	2	3	2	6	1	36	7	21	π b.
B–π^*_{v}	47	−0.24620	1	10	3	7	7	51	1	10	π b.
$\pi^*_{h/v}$	46	−0.26345	11	4	8	8	4	48	3	4	pseudo σ b.
π^*_{h}–$d_{x^2-y^2}$	44	−0.28585	8	16	9	7	3	46	1	4	σ b.
p_σ/π^*_{h}–d_{xy}	41	−0.33821	9	1	9	10	2	6	37	10	σ b.
π_{v}	40	−0.35322	5	6	10	17	1	24	13	7	n.b.
π_{v}	39	−0.35762	5	5	13	12	3	40	1	2	n.b.
π_{v}	38	−0.36579	4	9	7	11	3	28	18	4	n.b.
p_σ/π^2_{h}–d_{z^2}	36	−0.39215	9	3	10	5	0	48	2	1	n.b.
p_σ/π^2_{h}–d_{σ}	35	−0.40351	3	9	9	10	2	33	6	0	n.b.
π_{v}–d_{xz}/d_{yz}	34	−0.40717	16	9	10	14	2	38	2	1	n.b.
p_σ/π^2_{h}	31	−0.44130	1	1	10	9	1	10	25	0	n.b.
p_σ/π^2_{h}	29	−0.45284	2	3	9	10	6	14	16	0	n.b.
p_σ/π^1_{h}	27	−0.47845	2	4	23	22	0	16	2	13	σ b.
p_σ/π^1_{h}	25	−0.48458	2	1	4	5	1	53	1	2	σ b.

[a] Only selected orbitals are listed. [b] N_t is the terminal nitrogen and N_b the bridging nitrogen atom of the dinitrogen ligand. [c] The charge decomposition gives the sum of all corresponding atoms. [d] N_{AD} is the nitrogen atom of the NH_2 group. [e] a.b. = antibonding; n.b. = nonbonding; b. = bonding between the terminal nitrogen and boron atoms.

orbitals of the metal centers. This orbital, which forms two π bonds between the dinitrogen ligand and the two metal atoms, is quite similar to the HOMO obtained for model **I** (Figure 1). Additionally it has a small contribution on the boron atom, which is antibonding with respect to the terminal nitrogen atom. The corresponding nitrogen–boron bonding combination of this orbital is found in MOs ⟨48⟩ and ⟨47⟩, corresponding to a π bond between the terminal nitrogen and the Lewis acid (see Figure 10). Orbitals ⟨50⟩ and ⟨46⟩ represent a degenerate orbital deriving from the π^*_h and π^*_v orbital of the dinitrogen unit. These orbitals form a π (⟨50⟩) and a pseudo-σ (⟨46⟩) bond, respectively, between the nitrogen and the boron atoms. The interaction between the π^*_h orbital and $d_{x^2-y^2}$ (π^*_h–$d_{x^2-y^2}$; ⟨44⟩) results in two σ bonds between N5/N6 and Ta1 and one π bond between N5 and Ta2, similar to that found in model system **I**. Additionally, this orbital has small contribution from the boron atom that interacts with the nitrogen atom to form a pseudo-σ bond.

Importantly, the π and σ bonding orbitals of the dinitrogen unit interact with the tantalum d orbitals and the boron ligand as well. Specifically, the p_σ orbital and the π_h orbital of the dinitrogen unit mix to form the two combinations p_σ/π^1_h and p_σ/π^2_h (see Figure 10). The component p_σ/π^1_h, which is distributed over three orbitals (⟨41⟩, ⟨27⟩, and ⟨25⟩) forms a σ bond between the terminal nitrogen and boron atoms. These orbitals have the largest contribution both from the dinitrogen ligand and the boron atom and, therefore, represent the major interaction between nitrogen and boron. In contrast, the other combination p_σ/π^2_h as present in orbitals ⟨36⟩, ⟨35⟩, ⟨31⟩ and ⟨29⟩ has no contribution on the boron atom, but instead interacts with tantalum d-functions. The π_v orbital of the dinitrogen moiety does not show interaction with the boron atom either.

The LUMO and higher lying unoccupied orbitals have strong participation from tantalum d functions, corresponding to an approximate Ta^V configuration of **IVa** (d-shell empty). Since both back-bonding π* orbitals of the dinitrogen moiety are filled and are at lower energy than the manifold of d functions, an inverted bonding situation applies which is analogous to complex **1**. Table 6 compares the atomic charges (NPA) found for model system **I** with those calculated for models **II**, **III**, and **IVb** (model **IVb** is a more accurate model of complex **4** with the full $B(C_6F_5)_3$ group, cf. Experimental Section). In the inverted bonding scheme, up to four electrons are transferred from the metals to the π* orbitals of the dinitrogen group, which therefore gets strongly reduced. On the other hand, negative charge is withdrawn from N_2 by donation from the filled π orbitals to the empty metal d orbitals. In the case of **I**, the −4 charge

Table 6. NPA Charges of model systems **II**, **III** and **IVb** compared to model system **I**.

Atom	Charge **I**[b]	**II**	**III**	**IVb**
Ta1	1.42	1.46	1.47	1.50
Ta2	1.28	1.35	1.36	1.40
N5	−0.53	−0.52	−0.51	−0.53
N6	−0.55	−0.69	−0.72	−0.65
H[a]	−0.22	−0.21	−0.20	−0.19
$N_{AD}H_2$[a]	−0.41	−0.39	−0.39	−0.36
PH_3[a]	0.22	0.26	0.26	0.26
X	–	1.68	1.81	0.63
X-R_3[c]	–	−0.15	−0.15	−0.45

[a] Charge for each atom; charges are averaged. [b] Data taken from reference [15]. [c] R = Me for **II** and **III**; R = C_6F_5 for **IVb**.

of N_2 is thus decreased to −1.08 units, which are equally distributed over the two nitrogen atoms of N_2. In the Lewis acid adducts **2**–**4**, the negative charge on the dinitrogen ligand increases again, the additional charge being exclusively accumulated on the terminal nitrogen atom (−0.69, −0.72, and −0.65 for **II**, **III**, and **IVb**, respectively). As can be inferred from inspection of Table 6, this additional charge mostly derives from the metal centers, but also from the terminal N/P and bridging hydrido ligands.

Discussion

The formation of Lewis acid–base adducts with mononuclear transition-metal dinitrogen complexes is well known.[26–28] Generally these result from the addition of Lewis acidic species (Group 13 complexes or transition-metal complexes) to preformed mononuclear dinitrogen complexes. Alternatively, metallic reducing agents such as Mg are used to generate heterobimetallic dinitrogen complexes in which different levels of N_2 activation are observed. These compounds have been employed in salt metathesis schemes with other metal halides to provide entry into a variety of other heterobimetallic dinitrogen complexes.

Here it was shown that the side-on end-on dinitrogen complex $[\{(NPN)Ta\}_2(\mu\text{-}H)_2(\mu\text{-}\eta^1{:}\eta^2\text{-}N_2)]$ (**1**) reacts with the Lewis acids $GaMe_3$, $AlMe_3$, and $B(C_6F_5)_3$ to form the adducts $[\{(NPN)Ta\}_2(\mu\text{-}H)_2(\mu\text{-}\eta^1{:}\eta^2\text{-}NNGaMe_3)]$ (**2**), $[\{(NPN)Ta\}_2(\mu\text{-}H)_2(\mu\text{-}\eta^1{:}\eta^2\text{-}NNAlMe_3)]$ (**3**), and $[\{(NPN)Ta\}_2(\mu\text{-}H)_2\{\mu\text{-}\eta^1{:}\eta^2\text{-}NNB(C_6F_5)_3\}]$ (**4**). These compounds are somewhat anticipated by an earlier report of a trinuclear N_2 complex of titanium,[29] but the uncertainties in characterization and synthesis of this species are in marked contrast to the ready availability of **1** upon nitrogenation of $[\{(NPN)Ta\}_2(\mu\text{-}H)_4]$ and the controlled fashion in which **1** reacts with a variety of electrophiles. The outcomes of these reactions seem to exist in two broad classes; those that result from addition reactions and those that result from Lewis acid–base interactions. The former are often unstable to elimination of H_2 and further transformations including N−N bond cleavage, while the latter are surprisingly stable. This suggests that heterotrimetallic complex formation with **1** may offer new opportunities to transfer atoms and groups from this third metal center onto the dinitrogen fragment. In cases in which an addition reaction occurs it seems the H−E or X−E bond polarity must be suitable.

The solid-state molecular structures of the Lewis adducts **2**–**4** were determined by X-ray crystallography. The metric parameters of the Ta_2N_2 moiety are similar to those of the parent complex **1**, apart from the N−N distance which has increased from 1.319(4) Å (**1**) to 1.356(18), 1.363(7) and 1.393(7) Å, in **2**, **3**, and **4** respectively (cf Table 1). This indicates an increase of dinitrogen activation parallel to the Lewis acidity of the coordinated Group 13 complex. The aluminum and gallium atoms in **2** and **3** are clearly four-coordinate and trigonal pyramidal. Both the solid-state structure and the ^1H and $^{31}P\{^1H\}$ NMR spectra of **2** and **3** are very similar. The Ga−N bond is 0.108 Å longer than the Al−N bond, as expected. Attempts to prepare the BMe_3 or BEt_3 adducts were unsuccessful, but $B(C_6F_5)_3$ forms the adduct **4** despite the considerable steric bulk imposed by the three pentafluorophenyl groups. This demonstrates the accessibility of the terminal nitrogen atom of **1** to other reagents.

As evidenced by variable-temperature ^1H NMR spectroscopy, complexes **2**–**4** are fluxional in solution. In the high-temperature limit all display C_s symmetry, whereas C_1 symmetry is observed at lower temperatures. The transition temperatures are 320, 240, and 340 K for **2**, **3**, and **4**, respectively. The interconversion likely involves a "rocking" of the NPN ligands, such that the P-Ta-Ta-P angles sweep through 180°. Moreover, the vibrational spectroscopic properties of complexes **2**–**4** were determined. Vibrational spectroscopic data (resonance Raman/IR) were evaluated by normal coordinate analysis with the help of DFT calculations, allowing us to correlate the spectroscopic properties of **2**–**4** with their electronic structures.

The vibrational properties of **2**–**4** were found to be similar to those of **1**. The N−N stretching frequency is slightly decreased relative to **1**, in agreement with the elongation of the N−N bond. In contrast, the frequency of the metal/end-on dinitrogen vibration $\nu(Ta2\text{-}N_2)$ is found to increase significantly, shifting from a single peak at 656 cm^{-1} in **1** to a cluster of bands at around 700, 740, and 880 cm^{-1} in the Raman spectra of complexes **2**, **3**, and **4**, respectively. The frequencies of the metal/side-on dinitrogen vibrations remain approximately constant. Finally, the symmetric out-of-plane mode of the N_2 unit, which has not been observable in the spectra of **1**, was found at 256, 276, and 409 cm^{-1} in the spectra of complexes **2**, **3**, and **4**, respectively.

To evaluate the vibrational data, a QCB-NCA was applied. This method has been employed before in the vibrational study of compound **1**.[15] In this procedure, force constants and frequencies are calculated by DFT. Then selected force constants are fitted to the observed frequencies, all other force constants being fixed at their theoretical calculated values derived by the DFT calculation. A graphical representation of the force constants evaluated this way is given in Figure 11. The force constant for the N−N bond,

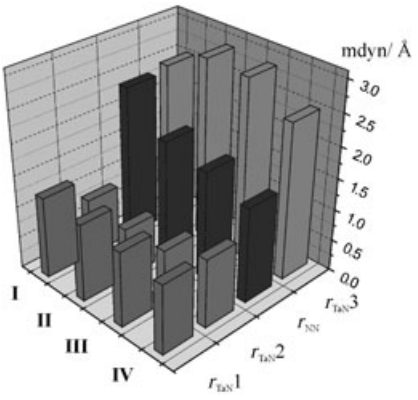

Figure 11. Evolution of M−N and N−N force constants.

which was calculated to 2.430 mdyn Å^{-1} in complex **1**, decreases in complexes **2**–**4** to 1.876 (**2**), 1.729 (**3**), and 1.515 mdyn Å^{-1} (**4**). This is in line with the trend of N–N bond lengths determined for complexes **1**–**4** (see above). In contrast, the tantalum/side-on nitrogen force constants $r_{TaN}1$ and $r_{TaN}2$ are at approximately the same values for complexes **1**–**4**. This should be expected by consideration of the metal–nitrogen bond lengths, which are quite similar in all four compounds.

The small decrease of N–N stretching frequencies observed for **2**–**4** relative to **1** appears to be in contrast to the significant decrease in force constants that occurs upon going from complexes **1** to **4**. This is explained by the fact that both N atoms of the N_2 unit oscillate against metal centers in the Lewis adducts (as opposed to the parent complex **1**), causing an increase of the N–N vibrational energy that acts against the decrease due to the lengthening of the N–N bond. As a result, the N–N force constants markedly decrease from complexes **1** to **4**, whereas ν(N–N) is only slightly reduced. The metal/end-on dinitrogen stretching frequency, on the other hand, increases monotonously relative to **1** in compounds **2**, **3**, and **4** by 84, 88, and 227 cm^{-1}, respectively, whereas the corresponding force constant shows a mixed behavior; that is, it increases in **2** and **3** and decreases in **4** with respect to **1**. Remarkably, the highest frequency of ν(Ta2-N_2) is observed for **4**, for which the corresponding metal–N force constant, $r_{TaN}3$, is smallest. Again, this is due to the fact that the dinitrogen unit oscillates against the Lewis acid in ν(Ta2-N_2), such that the frequency of this vibration is highest in complex **4**, which is coordinated to the Lewis acid with the highest mass and the strongest bond to the terminal nitrogen atom.

The electronic structure of the Lewis acid adducts is described on the basis of a hypothetical BH_3 adduct of **1** (**IVa**), providing a generic model of complexes **2**–**4**. The electronic structure of complex **1** itself has been analyzed before in terms of interactions between the tantalum d orbitals and the MOs of the dinitrogen.[12,15] Here it is found that these interactions are quite similar in model **IVa**. Based on the electronic structure described of **1**, it was expected that the bonding interactions between the terminal nitrogen and the Lewis acid atom would mostly involve the π_v^* and π_h^* orbitals of the dinitrogen unit, since these orbitals have strong contributions at the terminal nitrogen atom in **1** (see Figure 1). Based on the results obtained in the present study, this view has to be modified. Specifically it is found that the π_h and the p_σ orbital of the dinitrogen unit mix to form two hybrid orbitals (p_σ/π_h^1 and p_σ/π_h^2). The latter combination is N–B nonbonding, whereas the former combination is σ bonding with respect to boron and nitrogen. As evident from orbital analysis, this orbital mediates the strongest σ bond between the terminal nitrogen and boron atoms. In contrast, the π_v^* and π_h^* orbitals of N_2 exhibit much less interaction with the Lewis acid. Moreover, the π_v^*–d_{xz}/d_{yz} orbital, which is the HOMO ($\langle 51\rangle$) of model **IVa** interacts with the boron atom in a π antibonding fashion. This interaction, however, is quite weak as the boron contribution to this orbital is small (5%). The corresponding π bonding combinations are found in the B–π_v^* orbitals $\langle 48\rangle$ and $\langle 47\rangle$. Additionally, π_v^* mixes with π_h^* to form two $\pi_{h/v}^*$ hybrid orbitals ($\langle 50\rangle$ and $\langle 46\rangle$), which result in π and pseudo-σ bonding between the nitrogen and boron atoms, respectively. The π_h^*–$d_{x^2-y^2}$ orbital ($\langle 44\rangle$) also exhibits a σ bonding interaction with the Lewis acid. Thus, apart from the negligible π antibonding interaction of the HOMO, the π_v^* and π_h^* orbitals of the dinitrogen unit in fact form π and σ bonds with the boron atom. These interactions, however, are weak with respect to the dominant σ bond mediated by the p_σ/π_h hybrid orbital.

The NPA charges calculated for model **II**, **III**, and **IVb** of the adducts indicate that the negative charge on the dinitrogen ligand increases with respect to the model system **I**, although an electron-acceptor (Lewis acid) is bound. As further revealed by NPA, this additional charge on N_2 is mostly withdrawn from the tantalum center and is basically located at the terminal nitrogen atom. This continues a trend already observed and explained for **1**, that the charge transferred from the metal to N_2 mostly accumulates on the terminal N atom. The lengthening of the N–N bond observed upon coordination of the Lewis acids is therefore due to the fact that the electron density in the π* orbitals of the dinitrogen unit is increased, while electron density from the N–N bonding orbitals p_σ and π_h is withdrawn.

In summary, the accessibility of the terminal nitrogen atom of the side-on end-on N_2 coordinated complex **1** to external reagents has been demonstrated by the synthesis and characterization of the Lewis adducts **2**–**4**. A complete understanding of the spectroscopic properties of **2**–**4** has been achieved, and the vibronic differences to **1** have been explained. The electronic structure of the $Ta_2(\mu\text{-}\eta^1\text{:}\eta^2\text{-}N_2\text{-}X)$ (X = Lewis acid) moiety has been described and the activation of the dinitrogen ligand has been analyzed. Further spectroscopic and theoretical studies on derivatives of **1** resulting from addition of silanes and boranes should allow us to obtain insight into the ensuing reaction steps that will ultimately lead to cleavage of the N–N bond.

Experimental Section

Synthesis of 2, 3, and 4 and their ^{15}N-labeled derivatives: General synthetic methods and experimental conditions have been reported elsewhere.[13]

Synthesis of [{(NPN)Ta}$_2$(μ-H)$_2$(μ-η^1:η^2-N$_2$)] (1): Compound **1** and its ^{15}N-labeled derivatives were synthesized by literature methods.[12]

Synthesis of [{(NPN)Ta}$_2$(μ-H)$_2$(μ-η^1:η^2-NNGaMe$_3$] (2): Neat $GaMe_3$ (51 mg, 0.447 mmol) was added as a single portion to a solution of **1** (564 mg, 0.447 mmol) in toluene (20 mL). The compounds reacted immediately upon agitation, as demonstrated by an immediate colour change to yellow-brown. The solvent was removed under vacuum after 8 h, and the residues were triturated under hexanes, giving a brown solid. This solid was rinsed with minimal cold hexanes and dried, to yield complex **2** as a dark brown solid (591 mg, 96%). ^{1}H NMR (C_6D_6, 30 °C, 500 MHz): $\delta = -0.45$ (s, 15H; 9Ga(CH_3)$_3$, 6SiCH_3), −0.45, −0.12, −0.18, (s, 6H each, 18H total; SiCH_3), 0.73 (AMX, $^2J_{HH} = 13.8$, $^2J_{HP} = 10.8$, 4H; SiCH_2P), 1.43 (AMX, $^2J_{HH} = 14.1$, $^2J_{HP} = 12.2$, 4H; SiCH_2P), 6.90 (d, 2H; $^2J_{HP} = 6.2$ Hz, PPh *o-H*), 7.72 (d, 2H; $^2J_{HP} = 7.0$ Hz, PPh *o-H*) 7.19 (m,

2H; PhH), 7.08 (d, 4H; NPh *o*-H), 7.10–7.27 (m, 18H; PhH), 10.91 ppm (br, 2H; TaH); ^{13}C NMR (C_7D_8, 125 MHz, 25 °C): δ = 0.17 (br s, Ga(CH_3)$_3$) 0.82, 1.04, 2.27, 4.68 (SiCH_3) 22.09 (d), 31.76 (d) (SiCH_2P) 133.63 (d), 134.64 (d) (P-*Ph ipso*) 131.62, 130.84 (P-*Ph ortho*) 122.68, 129.43 ppm (N or P-*Ph*) (additional resonances occluded by solvent); ^{31}P{^{1}H} NMR (C_6D_6, 20 °C, 202 MHz): δ = 18.8 (d, $^3J_{PP}$ = 22.9 Hz, 1P), 10.1 ppm (d, J_{PP} = 22.9 Hz, 1P); elemental analysis calcd (%) for $C_{51}H_{73}GaN_6P_2Si_4Ta_2$: C 44.51, H 5.35, N 6.11; found: C 44.20, H 5.37, N 6.01.

Synthesis of [$^{15}N_2$]-2: The ^{15}N-labeled analogue was prepared from [$^{15}N_2$]-**1** in a manner similar to the preparation of **2** described above. ^{15}N NMR (C_7D_8, 299 K): δ = −29.9 (dd, $^1J_{NN}$ = 18.3 Hz, $^2J_{NP}$ = 27.5 Hz), 79.9 ppm (d, $^1J_{NN}$ = 18.3 Hz, $^2J_{NP}$ = 9.2 Hz); ^{31}P{^{1}H} NMR (C_7D_8, 299 K): δ = 18.8 (d, $^3J_{PP}$ = 23.0 Hz, $^2J_{PN}$ = 2.8 Hz , 1P), 10.0 ppm (1:2:1 triplet, $^3J_{PP}$ = 23.0 Hz, $^2J_{PN}$ = 25 Hz, couplings not well resolved, 1P).

Synthesis of [{(NPN)Ta}$_2$(μ-H)$_2$(μ-η^1:η^2-NNAlMe$_3$)] (3): A 2 M solution of $AlMe_3$ in toluene (1.0 mL, 2.0 mmol) was added to a solution of **1**, (1.06 g, 0.840 mmol) in toluene (20 mL). The solution immediately reacted, as demonstrated by an immediate colour change to a dark brown. The solvent was removed under vacuum, and toluene (10 mL) was added and then the sample dried again to remove excess $AlMe_3$. The remaining solid was rinsed with minimal cold hexanes and dried, to yield complex **3** as a pale brown solid (1.06 g, 95 %). ^{1}H NMR (C_6D_6, 30 °C, 500 MHz): δ = −0.47 (s, 9H; Al(CH_3)$_3$), −0.41, −0.30, −0.23, −0.04, 0.01, 0.04, 0.09, 0.10 (s, 24H total; SiCH_3), 0.65 (AMX, $^2J_{HH}$ = 13.5, $^2J_{HP}$ = 10.6, 2H; SiCH_2P), 1.48 (AMX, $^2J_{HH}$ = 13.5, $^2J_{HP}$ = 12.2, 2H; SiCH_2P), 1.59, 1.59 (m, 4H total; SiCH_2P), 6.74 (m, 2H; PhH), 6.83 (b, 2H; PPh *o*-H), 6.89 (m, 2H; PhH), 6.91 (d, 4H; NPh *o*-H), 7.10–7.27 (m, 18H; PhH), 8.24 (m, 2H; PPh *o*-H), 10.85 ppm (dd, $^2J_{HP}$ = 20.3, 14.3, 2H; TaH); ^{13}C NMR (C_6D_6, 20 °C, 125 MHz): δ = −7.94 (s, Al(CH_3)$_3$), −3.97, −0.25, −0.01, 3.71 (SiCH_3) 28.73 (d), 30.55 (d) (SiCH_2P) 133.47 (d), 132.58 (d) (P-*Ph ipso*) 130.52 129.81 (P-*Ph ortho*) 128.10, 128.02, 127.84, 127.76, 125.17, 124.82, 124.35 ppm (N or P-*Ph*); ^{31}P{^{1}H} NMR (C_6D_6, 20 °C, 202 MHz): δ = 18.9 (d, $^3J_{PP}$ = 22.9 Hz, 1P), 10.0 ppm (d, J_{PP} = 22.9 Hz, 1P); elemental analysis calcd (%) for $C_{51}H_{73}AlN_6P_2Si_4Ta_2$: C 45.94, H 5.52, N 6.30; found: C 46.20, H 5.47, N 6.00.

Synthesis of [$^{15}N_2$]-3: The ^{15}N-labeled analogue was prepared from [$^{15}N_2$]-**1** in a manner similar to the preparation of **3** described above. ^{15}N NMR (C_6D_6, 299 K): δ)−33.1 (dd, $^1J_{NN}$ = 18.8 Hz, $^2J_{NP}$ = 25 Hz), 54.6 ppm (d, $^1J_{NN}$ = 18.8 Hz, $^2J_{NP}$ = 8.4 Hz); ^{31}P{^{1}H} NMR (C_6D_6, 299 K): δ = 19.1 (d, $^3J_{PP}$ = 23.0 Hz, $^2J_{PN}$ = 8.4 Hz, $^2J_{PN}$ = 2.8 Hz , 1P), 10.0 ppm (d, $^3J_{PP}$ = 23.0 Hz, $^2J_{PN}$ = 25 Hz, $^3J_{PN}$ = 2.0 Hz, 1P).

Synthesis of [{(NPN)Ta}$_2$(μ-H)$_2${μ-η^1:η^2-NNB(C$_6$F$_5$)$_3$}] (4): Solid B(C_6F_5)$_3$ (0.3065 g, 0.5674 mmol, 0.95 equivalents) was added to a solution of **1** (0.7551 g, 0.5987 mmol) in C_6H_6 (20 mL). The solution immediately darkened and both the ^{31}P{^{1}H} and ^{1}H NMR spectra indicated that a reaction had occurred. Over 48 h brown benzene-insoluble needles precipitated. The solid was collected and dried, to yield **4**·0.5 C_6H_6 (0.998 g, 92 %). The co-crystallized benzene could not be removed under vacuum, and its presence was confirmed in the ^{1}H NMR spectrum and crystal structure. Alternatively, preparation in toluene followed by evaporation and trituration under hexanes afforded **4** free of benzene in similar yield. ^{1}H NMR (500 MHz, C_4H_8O, 240 K): δ = −0.67, −0.64, −0.57, −0.12, 0.18, 0.21, 0.53, 0.55 (s, 24H total; SiCH_3), 0.46, 1.26, 1.49, 1.66, 1.71, 1.83, 1.99, 2.28 (AMX, 8H total; CH_2 ring), 4.95 (br, 2H; phenyl protons), 5.77 (m, 1H; phenyl proton), 6.57 (d, 1H; NPh *o*-H), 6.67 (m, 1H; phenyl proton), 6.77 (overlapping multiplets, 3H; phenyl protons), 6.85 (d, 2H; NPh *o*-H), 7.03 (overlapping multiplets, 8H; phenyl protons), 7.11 (m, 2H; phenyl protons), 7.21 (d, 2H; NPh *o*-H), 7.33 (s, 3H; C_6H_6), 7.34 (overlapping multiplets, 3H; phenyl), 7.40 (m, 1H; phenyl protons), 7.73 (overlapping multiplets, 5H; phenyl protons and PPh *o*-H), 7.82 (m, 2H; PPh *o*-H), 11.36 (ddd, $^2J_{HH}$ = 16.3 Hz, $^2J_{HP}$ = 19.4, $^2J_{HP}$ = 25.7, 1H; TaH), 11.68 ppm (m, 1H; TaH); ^{31}P{^{1}H NMR (C_4H_8O, 240 K): δ = 11.6 (d, $^2J_{PP}$ = 23.9, NPN ligand), 17.7 ppm (br d, $^2J_{PP}$ = 23.9, NPN ligand); elemental analysis calcd (%) for $C_{66}H_{62}BF_{15}N_6P_2Si_4Ta_2$·0.5 C_6H_6: C 45.78, H 3.62, N 4.64; found: C 45.47, H 3.76, N 4.69.

Synthesis of [$^{15}N_2$]-4: The ^{15}N-labeled analogue of **4** was prepared from [$^{15}N_2$]-**1** in a manner identical to the preparation of **4** described above. ^{15}N{^{1}H} NMR (C_4D_8O, 299 K): δ = −21.2 (dd, $^1J_{NN}$ = 15.3 Hz, $^2J_{NP}$ = 22.0 Hz), 2.4 ppm (d, $^1J_{NN}$ = 15.3 Hz).

Test for reversibility of adduct formation: A mixture of [$^{15}N_2$]-**1** and natural abundance **2**, **3**, and **4** was dissolved in C_6D_6 and observed by ^{31}P{^{1}H} NMR spectroscopy. No coupling patterns typical of [$^{15}N_2$]-**2**, [$^{15}N_2$]-**3**, or [$^{15}N_2$]-**4** were observed even after three days at room temperature.

Single-crystal X-ray structure determination: Details of the structure determination are given below. Selected bond lengths and angles are given in Table 2.

[{(NPN)Ta}$_2$(μ-H)$_2$(μ-η^1:η^2-NNGaMe$_3$)] (2): Crystals of **2** suitable for X-ray diffraction analysis were obtained from a solution of **2** in benzene layered with hexamethyldisiloxane at ambient temperature in a glove box. Brown monoclinic crystal, dimensions 0.10 × 0.08 × 0.04 mm, space group $P2_1$, a = 11.4504(8), b = 22.9361(15), c = 22.6842(16) Å, β = 95.7563(2)°, V = 5870.6(7) Å^3, ρ_{calcd} = 1.555 g cm^{-3}, $2\theta_{max}$ = 60.1°. Measurements were made with an ADSC CCD area detector coupled on a Rigaku AFC7 diffractometer with graphic monochromated $Mo_{K\alpha}$ radiation (λ = 71069 Å) at −75 ± 1 °C in 0.50° oscillations with 15.0 s exposures by using φ oscillations from 0.0 to 190.0° at ξ = −90°. 44384 reflections were collected; 22490 were unique; equivalent reflections were merged. Data were collected and processed using d*TREK Area Detector Software, Version 4.13.[30] Structure solved by heavy-atom Patterson methods by using the programs DIRDIF94[31] and PATTY,[32] refined (11585 reflections, 1085 variables) as full-matrix least-squares against $|F^2|$ with SHELX97.[33] Residuals (refined on F, [I > 2.00σ(I)]): R_1, 0.059, wR_2 0.147.

[{(NPN)Ta}$_2$(μ-H)$_2$(μ-η^1:η^2-NNAlMe$_3$)] (3): Crystals of **3** suitable for X-ray diffraction analysis were obtained from a solution of **3** in toluene by slow evaporation at −60 °C in a glove box freezer. Brown triclinic crystal, dimensions 0.30 × 0.04 × 0.02 mm, space group $P\bar{1}$, a = 11.566(2), b = 23.596(3), c = 24.601(10) Å, α = 105.937(1), β = 95.508(1), γ = 94.284(1)°, V = 6390.2(22) Å^3, ρ_{calcd} = 1.482 g cm^{-3}, $2\theta_{max}$ = 56.0°. Measurements were made with a standard Siemens SMART CCD area detector system equipped with a normal focus molybdenum-target X-ray tube operated at 2.0 kW (50 kV, 40 mA) at −75 ± 1 °C in 0.30° oscillations with 60.0 s exposures by using φ oscillations from 0.0 to 190.0° at ξ = −90°. 38032 reflections were collected; 26874 were unique; equivalent reflections were merged. Data were processed using the Siemens SAINT program and corrected for absorption with the SADABS program.[34] Structure solved by direct methods and refined employing full-matrix least-squares on F^2 (Siemens, SHELXTL, version 5.04[35]) to a goodness of fit of 1.037 and final residuals of R_1 = 5.10 % [I > 2σ(I)], wR_2 = 9.66 % [I > 2σ(I)].

[{(NPN)Ta}$_2$(μ-H)$_2${μ-η^1:η^2-NNB(C$_6$F$_5$)$_3$}] (4): Crystals of **4** suitable for X-ray diffraction analysis were obtained from a solution of **4** in benzene layered with hexamethyldisiloxane at ambient temperature in a glove box. Orange-brown monoclinic crystal, dimensions 0.45 × 0.30 × 0.20 mm, space group $P2_1/n$, a = 24.8421(7), b = 24.330(5), c = 25.6475(2) Å, β = 99.795(4)°, V = 15423.5(4) Å^3, ρ_{calcd} = 1.628 g cm^{-3}, $2\theta_{max}$ = 61.0°. Measurements were made using an ADSC CCD area detector coupled with a Rigaku AFC7 diffractometer with graphic monochromated $Mo_{K\alpha}$ radiation (λ = 71069 Å) at −75 ± 1 °C in 0.30° oscillations with 8.0 s exposures by using φ oscillations from 0.0 to 189.9° at ξ = −90°. 143494 reflections were collected; 41721 were unique; equivalent reflections were merged. Data were collected and processed using d*TREK Area Detector Software.[30] Structure solved by heavy-atom Patterson methods using the programs DIRDIF92[31] and PATTY,[32] refined (22129 reflections, 1294 variables) as full-matrix least-squares against $|F^2|$ using SHELX97.[33] Residuals (refined on F, [I > 2.00σ(I)]): R_1, 0.055, wR_2 0.130.

CCDC-239836 (**2**), CCDC-240885 (**3**), and CCDC-239837 (**4**) contain the supplementary crystallographic data for this paper. These data can be obtained free of charge via www.ccdc.cam.ac.uk/conts/retrieving.html (or from the Cambridge Crystallographic Data Centre, 12 Union Road, Cambridge CB2 1EZ, UK; fax: (+44) 1223-336-033; or deposit@ccdc.cam.uk).

IR spectroscopy: Middle infrared (MIR) and far infrared (FIR) spectra were obtained from RbI pellets using a Bruker IFS 66v/S FTIR spectrometer. The resolution was set to 1 cm^{-1} for the MIR and 2 cm^{-1} for the FIR spectra.

Resonance Raman spectroscopy: Resonance Raman spectra were measured using a Dilor XY-Raman-spectrograph with triple monochromator and CCD detector. An Argon/Krypton mixed gas laser with a maximum power of 5 W was used for excitation. The spectra were recorded with an excitation wavelength of 568.2 nm. The samples were measured as KBr pellets and cooled to 10 K with a helium cryostat. Spectral bandpass was set to 2 cm^{-1}.

Normal coordinate analysis: Normal coordinate calculations were performed using the QCPE computer program 576.[36] The calculations were based on a general valence force field, and the force constants were refined using the nonlinear optimization routine of the simplex algorithm according to Nelder and Mead.[37] The models for the normal coordinate analysis were simplified by replacing the NPN ligand by NH_2 and PH_3 groups. In case of compound **4** the $B(C_6F_5)_3$ group was replaced by BH_3. The resulting model complexes **II**, **III** and **IVa** were optimized in C_1 symmetry, but with restrictions on the Ta-Ta-N-H dihedral angles. Model **IVb** is a more accurate model of complex **4** with the full $B(C_6F_5)_3$ group, leading to $[\{(PH_3)(NH_2)_2Ta(\mu\text{-}H)\}_2\{\mu\text{-}\eta^1\text{:}\eta^2\text{-}N_2\text{-}B(C_6F_5)_3\}]$, which was optimized in C_1 symmetry, also employing the above-mentioned restrictions on the Ta-Ta-N-H dihedral angles.

Frequencies and force constants (f-matrix) of these models were calculated. The hydrogen atoms of the NH_2 and PH_3 groups were removed to avoid artificial interactions and the masses of the hydrogen atoms of the BH_3 group of model **IV** were set to 167 for a better description of the huge pentafluorophenyl group in complex **4**. Finally, only selected force constants of the resulting f-matrix were refined according to the QCB-NCA procedure (see Results section).

Density functional theory calculations: Spin-restricted DFT calculations with Becke's three parameter hybrid functional with the correlation functional of Lee, Yang, and Parr (B3LYP)[38–40] were performed for the singlet ground state of simplified models of complexes **2**, **3**, and **4**. The LANL2DZ basis set was used for all calculations. It applies Dunning/Huzinaga full double zeta (D95) basis functions[41] on the first row and Los Alamos effective core potentials plus DZ functions on all other atoms.[42,43] Convergence was reached when the relative change in the density matrix between subsequent iterations was less than 1×10^{-8} for single points and optimizations. Charges were analyzed by using the natural bond orbital (NBO) formalism.[44–46] All computational procedures were used as they are implemented in the Gaussian 98 package.[47] Wavefunctions were plotted by using the visualization program Gaussview 2.1. The force constants in internal coordinates were extracted from the Gaussian output by using the program Redong.[48]

Acknowledgement

F.T. thanks DFG TU58–12 and FCI (Fonds der Chemischen Industrie) for financial support. F.S. thanks U. Cornelissen for assistance with the spectroscopic measurements. Acknowledgement is also made to NSERC of Canada for funding (Discovery grant to M.D.F. and Postgradute Scholarships to B.A.M. and S.A.J.).

[1] M. D. Fryzuk, S. A. Johnson, *Coord. Chem. Rev.* **2000**, *200–202*, 379–409.
[2] C. E. Laplaza, C. C. Cummins, *Science* **1995**, *268*, 861.
[3] D. V. Yandulov, R. R. Schrock, *Science* **2003**, *301*, 76.
[4] S. C. Lee, R. H. Holm, *Proc. Natl. Acad. Sci. USA* **2003**, *100*, 3595.
[5] F. Barriere, *Coord. Chem. Rev.* **2003**, *236*, 71.
[6] M. Hidai, Y. Mizobe, *Chem. Rev.* **1995**, *95*, 1115.
[7] M. Hidai, *Coord. Chem. Rev.* **1999**, *185/186*, 99–108.
[8] J. R. Dilworth, R. A. Henderson, A. Hills, D. L. Hughes, C. MacDonald, A. N. Stephens, D. R. M. Walton, *J. Chem. Soc. Dalton Trans.* **1990**, 1077.
[9] G. J. Leigh, *Acc. Chem. Res.* **1992**, *25*, 177.
[10] R. A. Henderson, *Transition Met. Chem.* **1990**, *15*, 330.
[11] M. D. Fryzuk, S. A. Johnson, S. J. Rettig, *J. Am. Chem. Soc.* **1998**, *120*, 11024–11025.
[12] M. D. Fryzuk, S. A. Johnson, B. O. Patrick, A. Albinati, S. A. Mason, T. F. Koetzle, *J. Am. Chem. Soc.* **2001**, *123*, 3960–3973.
[13] M. D. Fryzuk, B. A. MacKay, S. A. Johnson, B. O. Patrick, *Angew. Chem.* **2002**, *114*, 3861–3864; *Angew. Chem. Int. Ed.* **2002**, *41*, 3709–3712.
[14] M. D. Fryzuk, B. A. MacKay, B. O. Patrick, *J. Am. Chem. Soc.* **2003**, *125*, 3234–3235.
[15] F. Studt, B. A. MacKay, M. D. Fryzuk, F. Tuczek, *J. Am. Chem. Soc.* **2004**, *126*, 280–290.
[16] F. Studt, L. Morello, N. Lehnert, M. D. Fryzuk, F. Tuczek, *Chem. Eur. J.* **2003**, *9*, 520–530.
[17] J. Chatt, R. H. Crabtree, E. A. Jeffery, R. L. Richards, *J. Chem. Soc. Dalton Trans.* **1973**, 1167.
[18] J. Chatt, R. H. Crabtree, R. L. Richards, *J. Chem. Soc. Chem. Commun.* **1972**, *9*, 534.
[19] H. -S. Sun, X. -M. Wang, X. -Z. You, *Polyhedron* **1995**, *14*, 2159.
[20] D. J. Parks, W. E. Piers, M. Parvez, R. Atenico, M. J. Zaworotko, *Organometallics* **1998**, *17*, 1369.
[21] D. J. Parks, W. E. Piers, *J. Am. Chem. Soc.* **1996**, *118*, 9440.
[22] D. Rottger, G. Erker, R. Fröhlich, S. Kotila, *J. Organomet. Chem.* **1996**, *518*, 17.
[23] D. C. Bradley, M. B. Hursthouse, M. Motevalli, D. H. Zheng, *J. Chem. Soc. Chem. Commun.* **1991**, 7.
[24] D. C. Bradley, I. S. Harding, A. D. Keefe, M. Motevalli, D. H. Zheng, *J. Chem. Soc. Dalton Trans.* **1996**, 3931.
[25] H. Jacobsen, H. Berke, S. Doring, G. Kehr, G. Erker, R. Fröhlich, O. Meyer, *Organometallics* **1999**, *18*, 1724.
[26] Y. Mizobe, Y. Yokobayashi, H. Oshita, T. Takahashi, M. Hidai, *Organometallics* **1994**, *13*, 3764–3766.
[27] M. B. O'Donoghue, W. M. Davis, R. R. Schrock, W. M. Reiff, *Inorg. Chem.* **1999**, *38*, 243–252.
[28] H. Ishino, T. Nagano, S. Kuwata, Y. Yokobayashi, Y. Ishii, M. Hidai, *Organometallics* **2001**, *20*, 188–198.
[29] G. P. Pez, P. Apgar, R. K. Crissey, *J. Am. Chem. Soc.* **1982**, *104*, 482–490.
[30] d*TREK Area Detector Software, Version 4.13, Molecular Structure Corporation (**1996–1998**).
[31] DIRDIF94: P. T. Beurskens, G. Admiraal, G. Beurskens, W. P. Bosman, R. de Gelder, R. Israel, and J. M. M. Smits, **1994**. The DIRDIF-94 program system, Technical Report of the Crystallography Laboratory, University of Nijmegen (The Netherlands).
[32] PATTY: P. T. Beurskens, G. Admiraal, G. Beurskens, W. P. Bosman, S. Garcia-Granda, R. O. Gould, J. M. M. Smits, C. Smykalla, **1992**. The DIRDIF program system, Technical Report of the Crystallography Laboratory, University of Nijmegen (The Netherlands).
[33] SHELX-97: G. M. Sheldrick, Program for Crystal Structure Refinement, University of Gottingen (Germany) **1997**.
[34] The SADABS program is based on the method of Blessing; see R. H. Blessing, *Acta Crystallogr. Sect. A* **1995**, *51*, 33.
[35] SHELXTL, Structure Analysis Program, version 5.04; Siemens Industrial Automation, Madison, WI, **1995**.
[36] M. R. Peterson, D. F. McIntosh, QCPE program 576, Quantum Chemistry Program Exchange, Department of Chemistry, Indiana University, Bloomington, IN, **1988**.
[37] J. A. Nelder, R. Mead, *Comput. J.* **1965**, *7*, 308.
[38] A. D. Becke, *Phys. Rev. A* **1988**, *38*, 3098.
[39] A. D. Becke, *J. Chem. Phys.* **1993**, *98*, 1372.
[40] A. D. Becke, *J. Chem. Phys.* **1993**, *98*, 5648.
[41] T. H. Dunning, Jr., P. J. Hay, in *Modern Theoretical Chemistry*, (Ed.: H. F. Schaefer III), Plenum, New York, **1976**.
[42] P. J. Hay, W. R. Wadt, *J. Chem. Phys.* **1985**, *82*, 270 and 299.
[43] W. R. Wadt, P. J. Hay, *J. Chem. Phys.* **1985**, *82*, 284.
[44] J. P. Foster, F. Weinhold, *J. Am. Chem. Soc.* **1980**, *102*, 7211.
[45] A. B. Rives, F. Weinhold, *Int. J. Quantum Chem. Quantum Chem. Symp.* **1980**, *14*, 201.
[46] A. E. Reed, R. B. Weinstock, F. Weinhold, *J. Chem. Phys.* **1985**, *83*, 735.
[47] Gaussian 98 (Revision A.11), M. J. Frisch, G. W. Trucks, H. B. Schlegel, G. E. Scuseria, M. A. Robb, J. R. Cheeseman, V. G. Zakrzewski,

J. A. Montgomery, Jr., R. E. Stratmann, J. C. Burant, S. Dapprich, J. M. Millam, A. D. Daniels, K. N. Kudin, M. C. Strain, O. Farkas, J. Tomasi, V. Barone, M. Cossi, R. Cammi, B. Mennucci, C. Pomelli, C. Adamo, S. Clifford, J. Ochterski, G. A. Petersson, P. Y. Ayala, Q. Cui, K. Morokuma, D. K. Malick, A. D. Rabuck, K. Raghavachari, J. B. Foresman, J. Cioslowski, J. V. Ortiz, B. B. Stefanov, G. Liu, A. Liashenko, P. Piskorz, I. Komaromi, R. Gomperts, R. L. Martin, D. J. Fox, T. Keith, M. A. Al-Laham, C. Y. Peng, A. Nanayakkara, C. Gonzalez, M. Challacombe, P. M. W. Gill, B. G. Johnson, W. Chen, M. W. Wong, J. L. Andres, M. Head-Gordon, E. S. Replogle, J. A. Pople, Gaussian, Inc., Pittsburgh, PA, **2001**.

[48] A. Allouche, J. Pourcin, *Spectrochim. Acta Part A* **1993**, *49*, 571.

Received: June 25, 2004
Published online: November 24, 2004